FEATURE ARTICLE

Oxide nanowires for solar cell applications†

Qifeng Zhang, Supan Yodyingyong, Junting Xi, Daniel Myers and Guozhong Cao*

Oxide nanowire arrays were studied for their applications to solar cells. It was demonstrated that the nanowires could provide direct pathways for electron transport in *dye-sensitized solar cells* and therefore, while forming photoelectrode films, they offered better suppression of charge recombination than nanoparticles. However, the photoelectron films consisting of nanowires suffered a disadvantage in giving large surface area for dye adsorption. Such a shortcoming of nanowires had been exemplified in this paper illustrating that it could be well compensated by incorporating with nanoparticles to form a nanoparticle–nanowire array hybrid photoelectrode film. The oxide nanowires were also demonstrated to be able to enhance the performance of *inverted structure polymer solar cells* as a cathode buffer layer by establishing a large interface with the polymers so as to facilitate the transport of photogenerated electrons from the polymer to the electron collecting electrode. Such an enhancement effect could be further boosted while the nanowires were replaced with nanotubes; the latter may build up larger interface with the polymers than the former and therefore facilitates the electron transport more efficiently.

1. Introduction

Nanowires are a type of nanostructure with the dimensions in x and y axis directions much smaller than that in the z axis direction. Such a particularity in the structure has imparted nanowires with various applications in *electronic* and *optoelectronic devices*. For example, nanowires of Si, Ge, GaN and InAs present high electron mobility in view of a quasi-ballistic transport of electrons in the axial direction; the *field-effect-transistors* based on these nanowires show performance comparable to or even over the best reported for planar devices made from the same materials.[1–4] Nanowires for use in the generation of lasers have been also extensively reported over the past decade on the

Department of Materials Science and Engineering, University of Washington, Seattle, WA, 98195, USA. E-mail: gzcao@u.washington.edu
† This article was submitted as part of a collection highlighting papers on the 'Recent Advances in Semiconductor Nanowires Research' from ICMAT 2011.

Qifeng Zhang, PhD, is currently working at the University of Washington as a Research Assistant Professor. His research interests involve engineering applications of nanostructured materials on electrical devices including solar cells, UV light-emitting diodes (LEDs), field-effect transistors (FETs), and gas sensors. His current research focuses on the synthesis of nanomaterials and the application of nanomaterials in dye-sensitized solar cells (DSCs) and organic/inorganic hybrid solar cells. He has published over 100 papers and book chapters.

Qifeng Zhang

Guozhong Cao, PhD, is Boeing-Steiner Professor of Materials Science and Engineering and Adjunct Professor of Chemical and Mechanical Engineering at the University of Washington. He has published over 280 refereed papers and authored and edited 5 books including "Nanostructures and Nanomaterials". His current research is focused mainly on nanomaterials for energy conversion and storage including solar cells, lithium-ion batteries, supercapacitors, and hydrogen storage materials.

Guozhong Cao

nanowires of ZnO and GaN et al., which have an ideal geometry with one-dimensional structure that plays a role of waveguide and two parallel planes at the ends of individual nanowires that act as reflection mirrors, forming a microcavity that leads to amplified spontaneous emission and laser oscillation under an optical or electric pump.[5–11] Nanowires were also found to have important applications in *electrochemical devices* such as *lithium ion batteries* and *biosensors*.[12,13] Silicon nanowires have been demonstrated not to become fractured while being used for anode of a lithium ion battery.[14] Such a fracture usually happens to other silicon shapes when the lithium is drawn out of the silicon. Such a property enables the silicon nanowires to be a promising anode material that, in theory, can take up ten times more lithium than the carbon materials currently used. Besides silicon, other materials such as Ge,[15] $LiMn_2O_4$,[16] and V_2O_5[17] in the form of nanowires have been also observed to be advantageous in the intercalation/de-intercalation of lithium ions.

Besides the aforementioned applications, nanowires may also have important applications in the field of *photovoltaics*, in which the nanowires conducting electron transport and light trapping have been shown to be much superior to nanoparticles or planar thin film.[18–20] It was found that, in *dye-sensitized solar cells* (DSCs), the nanowires might provide direct pathways for electron conduction, leading to electron transport 100 times faster than in a typical nanoparticle-based solar cell.[18] Such an enhancement in electron conduction was attributed to the existence of an electric potential along the radial direction in the nanowires, sweeping the injected electrons to the inside of nanowires and thus facilitating the transport of electrons. The importance of direct pathways to the electron transport in a DSC with a photoelectrode made of nanowires is that the photogenerated electrons would no longer need to pass through a lot of boundaries that exist in the photoelectrode film made of nanoparticles in conventional DSCs, resulting in a reduced charge recombination, which occurs between the photogenerated electrons and those oxidized species (for example, I_3^-) in the electrolyte. However, compared to nanoparticles, nanowires are disadvantageous in providing sufficient internal surface area for dye adsorption while being used for DSCs. This severely limits the optical absorption and results in the power conversion efficiencies achieved by nanowires much lower than those record efficiencies (~10 to 11%) obtained for nanoparticles.[21]

In addition to playing a role in providing direct pathways for electron transport, compared to planar film, the nanowires also have the advantage in terms of lower reflective losses and being able to generate intensive light trapping, both of which contribute to enhancing the optical absorption of solar cells.[19,20] Garnett and Yang studied the light trapping in silicon nanowires.[20] It was found that the nanowires could strongly trap the incident light and have an extraordinary light-trapping path length enhancement factor as high as 73, which was far above the randomized scattering limit (~25) and was higher than those achieved with other light-trapping methods. Silicon nanowires have therefore been identified to be a promising material that might potentially create very high efficiency solar cells.

This paper summarizes our research on ZnO nanowires and TiO_2 nanorods for applications to *dye-sensitized solar cells* and *inverted structure polymer solar cells*. (Note that "*nanorods*" and "*nanowires*" are used interchangeably in this paper.) It will be

demonstrated that the internal surface area of a photoelectrode film made of a nanowire array can be increased by incorporating nanowires with nanoparticles, leading to a significant improvement in the dye adsorption and thus enhancing the power conversion efficiency of DSCs. For inverted structured polymer solar cells, the use of a nanowire array for the buffer layer may result in a branch structure that stretches into the polymer layers and accordingly facilitates the transport of photogenerated electrons by shortening the traveling distance of the photogenerated electrons in PCBM, which serves as the electron transporting layer in polymer solar cells. The facilitation of electron transport benefits the solar cells by increasing the electron collecting efficiency, resulting in the achievement of higher efficiency for the cells with a nanowire buffer layer than for those with a planar thin film. Our study would also demonstrate that the solar cell performance can be further boosted by employing nanotubes for the buffer layer. It is attributed to the fact that the nanobutes can provide an even larger specific surface area than the nanowires and, as a result, the interface established between the nanotube buffer layer and the polymers is larger than that established with the nanowires, leading to an increased opportunity for the photogenerated electrons to transport from the PCBM to the buffer layer, giving rise to more efficient electron collection.

2. Nanoparticle–nanowire array hybrid photoelectrodes for dye-sensitized solar cells

The nanoparticle–nanowire array hybrid structure was developed to increase the surface area of a DSC photoelectrode made of a nanowire array by filling up the gaps between the nanowires with nanoparticles and, meanwhile, retain the advantage of nanowires as direct pathways for electron transport.[22]

2.1 Fabrication and characterization of ZnO nanoparticle–nanowire array hybrid photoelectrode

ZnO nanowires were fabricated on a fluorine-doped tin oxide (FTO) glass substrate first. In a specific fabrication, a seed layer of ~100 nm thick ZnO nanocrystals was pre-prepared on the FTO glass substrate by spin-coating a solution of 0.6 M zinc acetate dihydrate in 2-methoxyethanol/monoethanolamine. The substrate with seed layer was annealed at 250 °C for 10 min and then soaked in an aqueous solution containing 0.015 M zinc nitrate and 0.015 M hexamethylenetetramine for the growth of a ZnO nanowire array at 95 °C for 60 h.[22,23] To ensure approximately constant concentration of the ZnO precursor, the growth solution was refreshed every 12 h. In a separate process, nanoparticles of ZnO were synthesized through hydrolysis of zinc acetate dihydrate in diethylene glycol (DEG) at elevated temperature, ~190 to 240 °C.[24] The resulting precipitate of ZnO nanoparticles was washed with ethanol several times through a repeated centrifuging and re-dispersion. A colloidal suspension of ZnO nanoparticles dispersed in ethanol was finally obtained. The nanoparticle–nanowire array hybrid photoelectrode film was obtained by spin-coating the as-prepared ZnO nanoparticle suspension on the ZnO nanowire array at relatively low speed.

Shown in Fig. 1 are the scanning electron microscope (SEM) images of the ZnO nanowire array before and after spin-coating with ZnO nanoparticles. It can be seen that the nanowires are
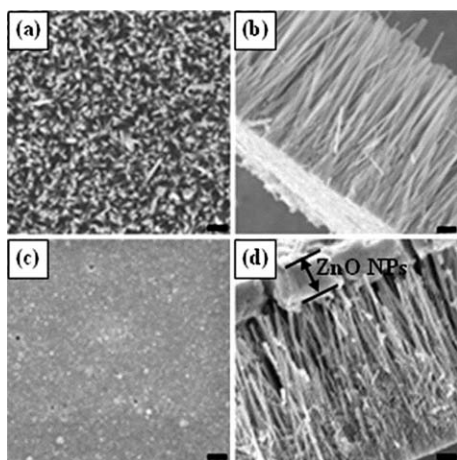
Fig. 1 SEM images of (a) top view of ZnO nanowire array, (b) cross-section of ZnO nanowire array, (c) top view of nanoparticle–nanowire array hybrid film, and (d) cross-section of nanoparticle–nanowire array hybrid film. Scale bars in (a–d) are 1 μm.[22]

vertically grown on the substrate with good alignment. The diameters of these nanowires range from 40 nm to 500 nm (average $\approx$ 116 nm), their length is approximately 11 μm, and the density of nanowires is estimated to be ~14 wires μm^{-2}. The spin-coating of ZnO nanoparticles, which possess an average diameter of 14 nm, leads to the formation of a ~2 μm thick cover layer of nanoparticles on the top of the nanowire array, as shown in Fig. 1d. Apart from the formation of a topping layer, it can also be seen that a small portion of nanoparticles penetrate into the gaps between the nanowires, yielding a combined structure with ZnO nanoparticles attached on the surface of nanowires.

The nanoparticle–nanowire array hybrid film was sensitized by soaking in a 0.5 M N3 dye solution for ~30 min. The solar cell device was assembled by employing the as-fabricated dye-sensitized nanoparticle–nanowire hybrid photoelectrode as an anode and a glass substrate coated with platinum film as a cathode to form a sandwich structure, and between these two electrodes (separated by a 40 μm thick spacer) a liquid electrolyte[24] was introduced as a medium to bridge the two electrodes and conduct the charges when the solar cell was under operating conditions. The power conversion efficiency was tested when the solar cells were irradiated by AM 1.5 simulated sunlight with a power density of 100 mW cm^{-2}.

2.2 Enhancing solar cell efficiency with nanoparticle–nanowire array hybrid photoelectrode

Fig. 2 compares the photovoltaic performance of the solar cells with a photoelectrode film made of (1) nanoparticles (ZnO NP) alone, (2) a nanowire array (ZnO NW) alone, and (3) a nanoparticle–nanowire array (ZnO NW–NP) hybrid. The detailed information and parameters of these solar cell samples are summarized in Table 1. For the photoelectrodes made of nanowires alone, one can see that the solar cell efficiency shows a dependence on the average length of the nanowires. As the nanowire length increases from 1.7 μm to 5.1 μm, the efficiency goes up from 0.94% to 1.16%. A further increase of the nanowire length to 11 μm leads to the achievement of 1.58% efficiency. Considering over 10% efficiencies reported for TiO$_2$
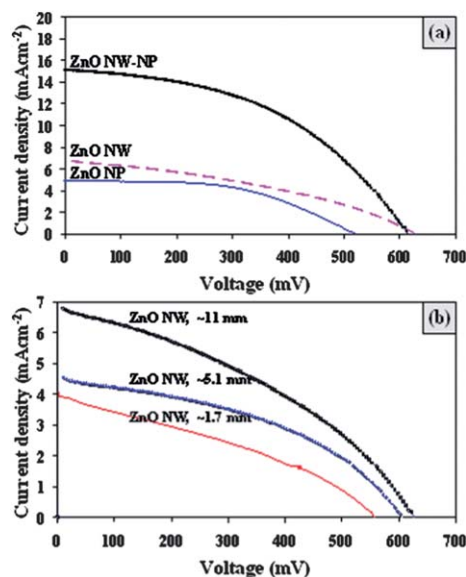
Fig. 2 (a) A comparison of solar cell performance of photoelectrodes made of ZnO nanoparticles (ZnO NP), ZnO nanowires (ZnO NW), and ZnO nanoparticle–nanowire array hybrid film (ZnO NW–NP). (b) Current–voltage (I–V) curves of ZnO nanowire photoelectrodes different in nanowire length.[22]

Table 1 Summary of DSC performance of photoelectrodes made of a ZnO nanowire array (ZnO NW), ZnO nanoparticles (ZnO NP), and ZnO nanoparticle–nanowire array hybrid film (Hybrid ZnO NW–NP). (J_{sc}: short-circuit current density, V_{oc}: open-circuit voltage, FF: fill factor, and η: power conversion efficiency)[22]

Sample	Thickness of photoelectrode film/μm	J_{sc}/mA cm^{-2}	V_{oc}/mV	FF (%)	η (%)
ZnO NW	~1.7 (NW)	4.09	553	41	0.94
ZnO NW	~5.1 (NW)	4.55	609	41	1.16
ZnO NW	~11 (NW)	6.79	629	37	1.58
ZnO NP	~10 (NP)	4.94	521	51	1.31
Hybrid ZnO NW–NP	~11 + ~2 (NW + NP)	15.16	613	46	4.24

nanoparticle-based solar cells, the obviously low efficiencies for ZnO nanowire photoelectrodes are first of all attributed to their very low internal surface area that results in insufficient dye adsorption and therefore poor optical absorption as well as low photocurrent density of the cells. However, simply increasing the nanowire length may not satisfyingly solve this problem. As shown in Table 1, while the nanowire length increases from 1.7 μm to 11 μm, which supposes to approximately increase the internal surface area by 5.5 fold, the photocurrent density increasing from 4.09 mA cm^{-2} to 6.79 mA cm^{-2} only shows an enhancement by ~1.7 fold. This indicates that an increase of the nanowire length may indeed yield a larger internal surface area of the photoelectrode film. However, this would also result in a longer distance for the injected electrons to transport within the nanowires and, therefore, increase the probability for electrons to be recombined with the oxidized species in the electrolyte or be trapped with the defects in the oxide. Such an increased recombination rate and trapping rate offset the contribution from

optical absorption enhancement owing to an increase in the length of nanowires as well as the dye adsorption amount. Therefore, the photocurrent density (or the solar cell efficiency) does not show a linearly proportional increase with the increasing nanowire length.

Another thing that is worthy of being addressed is that the efficiency of the ZnO nanoparticle photoelectrode, 1.31%, is lower than the 1.58% obtained for the ZnO nanowire photoelectrode when the film thicknesses of them are close to each other. Obviously, such an experimental observation conflicts with the assumption that the solar cells efficiency should be in proportion to the internal surface area of the photoelectrode film, since the internal surface area of the nanoparticle film is undoubtedly higher than that of the nanowire array film. A possible explanation for this phenomenon is that the dye adsorption of the ZnO nanoparticle photoelectrode film with pore size much smaller than that of a photoelectrode film comprised of nanowire array is far from optimization. This is because, unlike TiO$_2$, the ZnO is much less stable in a ruthenium-based dye solution. A reaction occurring between the surface atoms of ZnO and the dye molecules may lead to the formation of a Zn^{2+}/dye complex. Such a complex is inactive to the electron injection and therefore results in low power conversion efficiencies of ZnO-based DSCs.[25] Moreover, the formation of a Zn^{2+}/dye complex would further induce the aggregation of dye molecules on the surface of ZnO, which however obstructs the diffusion of electrolyte and hereby largely diminishes the solar cell performance.[26] For this reason, the sensitization of the ZnO photoelectrode film is usually adopted for a time period as short as 0.5–1 h, which is significantly different from the 8–24 h typical for the TiO$_2$ photoelectrode.[27] Considering that the ZnO nanoparticles employed in this study are ∼14 nm in diameter, the pore size of the film consisting of these ZnO nanoparticles is estimated to be on the scale of several nanometres. It is most likely that the dye molecules cannot achieve a complete penetration into the entire film in a very short sensitization time (e.g., ∼30 min) and therefore cannot form an ideal monolayer adsorption on the surface of ZnO nanoparticles. In this regard, the nanowire array film has a much more open structure than the nanoparticle film and therefore allows the dye solution to infiltrate into the film very quickly prior to the formation of a severe aggregation of dye. The ZnO nanowire array film was therefore observed to have higher efficiency than the nanoparticle film (Fig. 2 and Table 1).

The ZnO nanoparticles and nanowire array alone for the photoelectrode film only generated solar cell efficiencies at a relative low level, 1.31–1.58%. However, in our study it was found that a joint use of nanoparticles and nanowire array to form a hybrid structure photoelectrode may significantly increase the efficiency to as high as 4.24%. Such a hybrid structure photoelectrode boosting solar cell efficiency is attributed to the employment of ZnO nanoparticles that may greatly increase the internal surface area of the nanowire array photoelectrode film. Furthermore, the hybrid structure that is comprised of nanoparticles attached on the surface of nanowires (Fig. 3) allows the photogenerated electrons to transfer from the nanoparticles to the nanowires and then transport within the nanowires. This enables the electron transport and collection to be more efficient than in a photoelectrode film consisting of nanoparticles alone. To speak briefly, the nanoparticle–nanowire
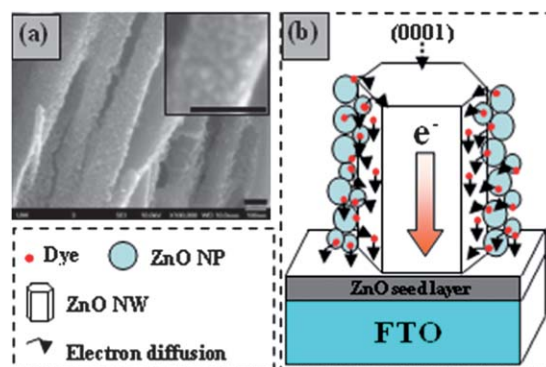
Fig. 3 ZnO nanoparticle–nanowire array hybrid photoelectrode for DSC. (a) Cross-sectional SEM images of ZnO nanowire array with ZnO nanoparticles adsorbed on the surface, and (b) schematic drawing showing the nanoparticle–nanowire array hybrid structure and the electron transfer from nanoparticles to nanowires and transport in the nanowires.[22]

array hybrid film is such a structure that integrates both the advantage of nanoparticles which provide large surface area and the advantage of nanowires which serve as highly efficient pathways for electron transport. In addition, from Fig. 1d, it can be seen that the hybrid photoelectrode film of the ZnO nanowire array filled up with ZnO nanoparticles remains a relatively open structure that allows a quick infiltration of the dye solution.

3. Application of nanowires (nanorods or nanotubes) in inverted structure polymer solar cells

Polymer solar cells are a type of photovoltaic device based on bulk heterojunction (BHJ) established with electron-donor materials such as poly(3-hexylthiophene) (P3HT) and electron-acceptor material such as [6,6]-phenyl-C$_{61}$-butyric acid methyl ester (PCBM). According to the difference in configuration, polymer solar cells can be classified as *conversional structure solar cells* and *inverted structure solar cells*.[28] The conventional polymer solar cells adopt a bottom-anode-top-cathode configuration as shown in Fig. 4a, where an anode buffer layer of poly(3,4-ethylene dioxythiophene) doped with poly(4-styrenesulfonate) (PEDOT:PSS) serving as a hole transporting material is deposited on a transparent conductive substrate such as ITO or FTO glass, followed by an active layer of mixture of P3HT and PCBM, and a cathode buffer layer of oxide thin film. A metal film as the electron-extracting electrode, i.e., the so-called cathode, is finally deposited. Under photoexcitation, the excitons generated in the active layer move to the interface of PCBM and P3HT, where the excitons get separated and dissociate into free carriers (i.e., holes and electrons) due to the offsets of molecular orbital energy levels (highest occupied molecular orbital, HOMO, and lowest unoccupied molecular orbital, LUMO) between the electron-donor material and the electron-acceptor material, which provide a driving force to overcome the exciton binding energy (around 0.3–0.5 eV).[29] After the exciton dissociation, the holes move toward the ITO side through the PEDOT:PSS hole transporting layer, i.e., anode buffer layer, which provides the P3HT electron-donor material with an ohmic contact. At the same time, the electrons go to the opposite
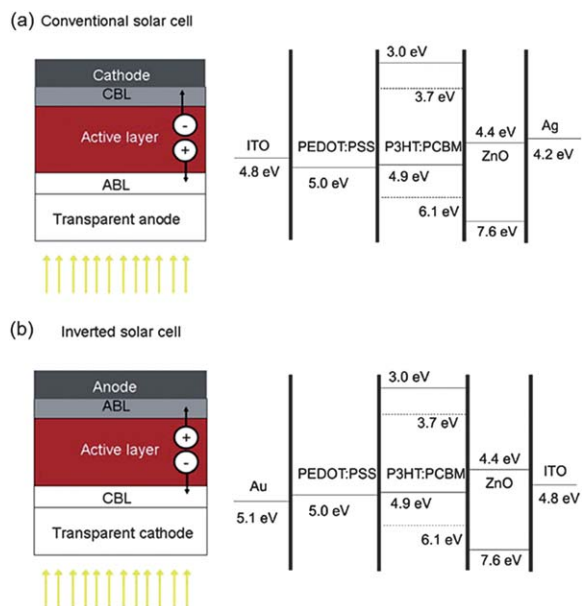
Fig. 4 Configurations and energy band structures of (a) conventional structure polymer solar cells and (b) inverted structure polymer solar cells. (ABL: anode buffer layer; CBL: cathode buffer layer.)[29,32]

direction toward the electron collecting electrode through the cathode buffer layer, which is an oxide film providing the PCBM electron-acceptor material with an ohmic contact and may transport electrons efficiently. Owing to newly developed materials such as PTB7 and $PC_{71}BM$, the polymer solar cells with a conventional structure have achieved efficiencies over 7% recently.[30] The conventional structure polymer solar cells, however, have demonstrated a severe disadvantage in chemical stability. It is because of (1) the ITO/PEDOT:PSS interface that is not chemically stable and has an adverse effect on the device performance over time,[31] and (2) the low work function metal such as aluminium (work function $\sim$4.2 eV) used in the conventional structure solar cells as the cathode, which is air-sensitive and degrades the solar cell performance very quickly.

The inverted structure polymer solar cells with a bottom-cathode-top-anode configuration were invented to overcome the stability problem of the conventional structure solar cells to some extent. In an inverted solar cell, the ITO substrate is coated by a layer of metal oxide so as to avoid the ITO/PEDOT:PSS interface. The active layer of P3HT/PCBM is prepared on the oxide film and then a PEDOT:PSS layer is fabricated prior to the deposition of the metal electrode (Fig. 4b). The excitons are also generated in the P3HT/PCBM active layer. However, unlike in the conventional structure solar cells where the holes move to the ITO side, the holes in the inverted solar cells move to the metal electrode side. Meanwhile, the electrons diffuse to the oxide cathode buffer layer, pass through it, and finally reach the ITO collecting electrode. The inverted structure solar cells benefit from their bottom-cathode-top-anode configuration. With such a configuration, on one hand, the ITO/PEDOT:PSS interface can be successfully avoided. On the other hand, since the metal electrode (*i.e.*, anode) is adjacent to the hole-transporting layer of PEDOT:PSS, a high work function metal such as gold is chosen to form an ohmic contact with the polymer (Fig. 4b). This is

another reason that a polymer solar cell with an inverted structure may have better environmental stability than that with a conventional structure.

The role of oxide film, which serves as a cathode buffer layer in the inverted structure polymer solar cells, has been suggested to separate the P3HT:PCBM active layer and the ITO collecting electrode so as to prevent the holes in the active layer from being recombined with the electrons in the ITO film.[29] Our study (shown later) points out that the structure and morphology of the oxide buffer layer may bring about a moderate influence on the solar cell performance. The use of an oxide nanorod array with a suitable nanorod length for the buffer layer can achieve solar cells with power conversion efficiency higher than that obtained for the cell with a thin film buffer layer. Our study also demonstrates that the nanorod array can be utilized as a template for the fabrication of nanotube array; the latter used as a cathode buffer layer for the inverted structure solar cells may generate higher efficiency than the former. The advantage of nanorod or nanotube array compared with a planar film is that the nanorods or nanotubes stretch into the polymers and may establish a larger interface with the PCBM polymer than the planar film. Such a large interface between the polymer and the cathode buffer layer may facilitate the transfer of photogenerated electrons from the PCBM to the electron collecting electrode. The higher charge mobility of oxide nanorods or nanotubes than that of PCBM is another aspect that makes a contribution to the solar cell performance by improving electron collecting efficiency.

3.1 TiO_2 nanorod array serving as the buffer layer

3.1.1 Fabrication and characterization of TiO_2 nanorod array. The TiO_2 nanorod array was fabricated on the FTO glass substrate by placing the substrate in an autoclave that contained a mixture solution of distilled water and hydrochloric acid in a volume ratio of 1 : 1, to which was added 5% (in volume) titanium butoxide.[33] The autoclave was then sealed and transferred to a furnace for hydrothermal reaction at 150 °C for 85 min (denoted as TiO_2 NRs 1) or 100 min (denoted as TiO_2 NRs 2). The TiO_2 nanorod array film grown on the FTO glass substrate was then rinsed with distilled water and finally underwent a thermal treatment at 450 °C for 1 h.[34]

The TiO_2 nanorod array films were characterized with SEM and XRD in terms of their morphology and crystal structure. The results are shown in Fig. 5. From the SEM images, it can be seen that the samples grown for different time periods present an obvious difference in nanorods' diameter and length. The nanorods with the growth time of 85 min (*i.e.*, TiO_2 NRs 1) show diameters of 50 $\pm$ 15 nm and length of $\sim$140 nm. For the nanorods with the growth time of 100 min (*i.e.*, TiO_2 NRs 2), the diameters and length increase to 75 $\pm$ 15 nm and $\sim$500 nm, respectively. The XRD analysis reveals that the TiO_2 nanorods synthesized with the as-described hydrothermal method possess a rutile phase.

3.1.2 Preparation of inverted structure polymer solar cells. The preparation of inverted structure solar cells involved a spin-coating of polymers on the TiO_2 nanorod arrays that were grown on the FTO glass substrate and then a vacuum-deposition of silver thin film as the top electrode, forming a device with the
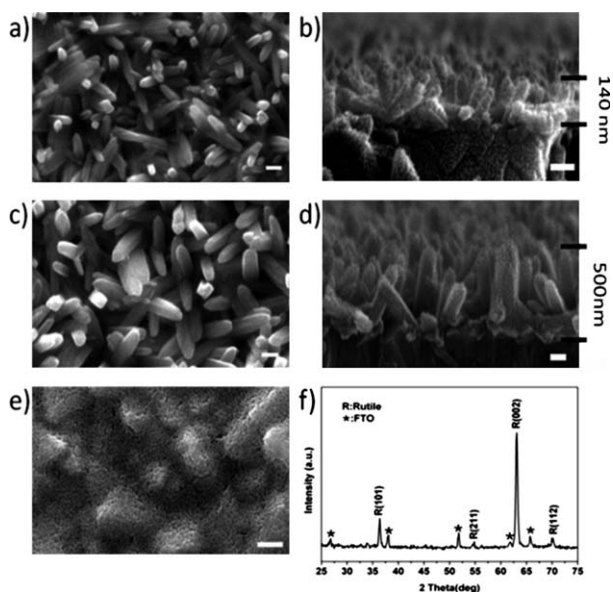
Fig. 5 Characterization of TiO$_2$ films deposited on the FTO glass substrate. (a and b) Top view and cross-sectional SEM images of TiO$_2$ nanorod array grown for 85 min (TiO$_2$ NRs 1), (c) and (d) for 100 min (TiO$_2$ NRs 2), respectively. (e) Top view SEM image of TiO$_2$ dense film, and (f) XRD pattern of TiO$_2$ nanorod array grown on FTO glass.[34]

FTO/TiO$_2$ nanorod array/PCBM/P3HT:PCBM/PEDOT:PSS/ Ag configuration, where the TiO$_2$ nanorod array served as the cathode buffer layer, P3HT and PCBM were the electron-donor and electron-acceptor, respectively, PEDOT:PSS was a hole-transporting layer, and Ag was the top electrode ~100 nm in thickness. During fabrication, the P3HT:PCBM active layer was achieved by spin-coating a mixture solution of 20 mg mL^{-1} P3HT and 16 mg mL^{-1} PCBM in chlorobenzene. A consequent thermal treatment at 225 °C for 1 min led to phase separation of the P3HT and PCBM. Prior to the deposition of Ag electrode, the sample was annealed at 120 °C for 10 min.

For comparison, another device was prepared with the same configuration but using a substrate coated with TiO$_2$ thin film instead of nanorods as the cathode buffer layer. The fabrication of the TiO$_2$ thin film involved a preparation of TiO$_2$ sol by adding 1 mL of titanium isopropoxide to 20 mL of distilled water containing 0.5 mL of hydrochloric acid and, then, a spin-coating of the sol on a FTO glass substrate. The film of TiO$_2$ was converted from the amorphous phase to the crystalline anatase phase through a thermal treatment of the substrate at 450 °C for 0.5–1 h.

3.1.3 Solar cell performance. Shown in Fig. 6a and Table 2 is the photovoltaic performance of the solar cells that employ a short TiO$_2$ nanorod array (TiO$_2$ NRs 1), a long TiO$_2$ nanorod array (TiO$_2$ NRs 2), and a TiO$_2$ dense film (TiO$_2$ DF), respectively, as the cathode buffer layer. It can be seen that the cell with the short TiO$_2$ nanorod array (i.e., TiO$_2$ NRs 1) achieves the highest efficiency, 3.21%. The efficiencies are 2.70% for the long TiO$_2$ nanorod array (i.e., TiO$_2$ NRs 2) and 2.97% for the TiO$_2$ thin film.

To understand the difference in solar cell efficiency arising from the cathode buffer layer that employs differently structured
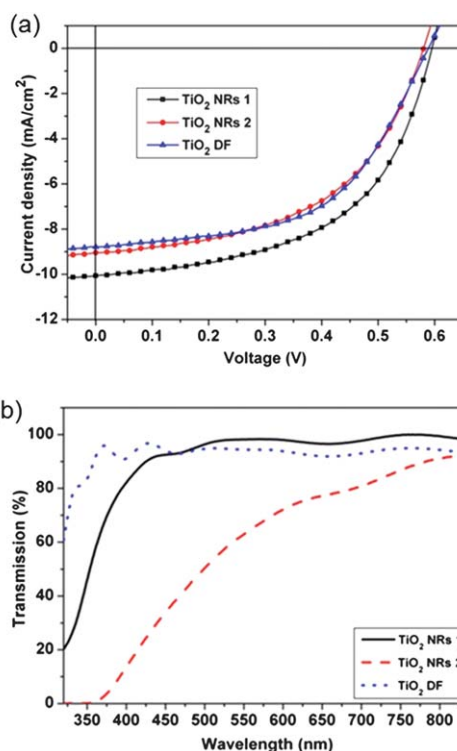
Fig. 6 Comparisons of (a) photovoltaic performance of inverted structure polymer solar cells using the TiO$_2$ nanorod array or thin film as the cathode buffer layer and (b) optical transmittance of FTO glass substrates coated with TiO$_2$ nanorod array or thin film. (TiO$_2$ NRs 1: 140 nm long TiO$_2$ nanorod array, TiO$_2$ NRs 2: 500 nm long TiO$_2$ nanorod array, TiO$_2$ DF: TiO$_2$ dense film.)[34]

Table 2 Summary of photovoltaic properties of inverted solar cells with cathode buffer layer of TiO$_2$ nanorod array or thin film. (TiO$_2$ NRs 1: 140 nm long TiO$_2$ nanorod array, TiO$_2$ NRs 2: 500 nm long TiO$_2$ nanorod array, TiO$_2$ DF: TiO$_2$ dense film)[34]

Sample	V_{oc}/mV	J_{sc}/mA cm^{-2}	FF	η (%)
TiO$_2$ NRs 1	595	10.06	0.536	3.21
TiO$_2$ NRs 2	580	9.05	0.513	2.70
TiO$_2$ DF	589	8.80	0.538	2.79

films, optical transmittance spectra of the TiO$_2$ nanorod arrays (TiO$_2$ NR 1 and TiO$_2$ NR 2) and TiO$_2$ thin film grown on the FTO glass substrate was measured. The results are shown in Fig. 6b. One can see that the short TiO$_2$ nanorod array (i.e., TiO$_2$ NR 1) presents the transmittance approximately in line with that of the TiO$_2$ thin film. Both of them show good transparency in the visible region. However, the long TiO$_2$ nanorod array (i.e., TiO$_2$ NR 2) indicates an apparently low transmittance over the ultraviolet and visible regions. This can be attributed to light scattering generated by the nanorod array film of the TiO$_2$ NR 2 sample consisting of nanorods ~75 nm in diameter and ~500 nm in length, the dimensions of which are comparable to the wavelengths of visible light. Such a light scattering reflects a portion of the incident light and results in a decrease in the transparency of the TiO$_2$ NR 2 nanorod array film.

What is very interesting is that the cell with a short nanorod array (~140 nm in length) as the cathode buffer layer (TiO$_2$ NR 1) has higher power conversion efficiency than the cell with a thin film (TiO$_2$ DF). A possible explanation is that the single crystalline TiO$_2$ nanorods synthesized *via* a hydrothermal method possess better crystallinity than the spin-coated polycrystalline TiO$_2$ thin film, *i.e.*, the former has less electron trapping than the latter, and therefore the electron transport in the nanorods is more efficient than in the thin film. This results in higher electron collecting efficiency as well as higher power conversion efficiency for the cell with a nanorod buffer layer compared to that with a thin film buffer layer. Note that the light scattering caused by short nanorods does not appreciably affect the optical transparency of the nanorod array film. Oversize nanorods would generate severe light scattering, which diminishes the optical transmittance and counteracts the contribution by single crystal nanorods that yield enhanced electron transport.

Besides the reason that the nanorods have better crystallinity than the thin film, another possibility of the enhanced solar cell performance is that the nanorod buffer layer may establish a larger interface with the polymers than a planar thin film buffer layer in view of the nanorods stretching into the polymers of P3HT:PCBM (Fig. 7). Such a branch structure as well as the large interface contributes to the solar cell by shortening the traveling distance of the photogenerated electrons in PCBM and facilitating the electrons to quickly transport out of the PCBM and get into the TiO$_2$ nanorods, followed by diffusion to the FTO collecting electrode. The solar cell efficiency is therefore enhanced since (1) a reduced traveling distance of photogenerated electrons in PCBM may decrease the recombination rate between the electrons in PCBM and the holes in P3HT, and (2) the semiconductor TiO$_2$ nanorods provide higher charge mobility than the PCBM, and therefore the electron collection is more efficient in TiO$_2$ nanorods (in the case of nanorod buffer layer) than in the PCBM polymer (in the case of thin film buffer layer).

However, our study regarding the use of TiO$_2$ tubes for the buffer layer (shown below) seems to support the second possibility more, *i.e.*, the large interface provided by the nanorods (or nanotubes) facilitating the electron collection is more likely to be the reason for the better performance of the solar cells with a nanorod array buffer layer compared with those using a planar thin film buffer layer.
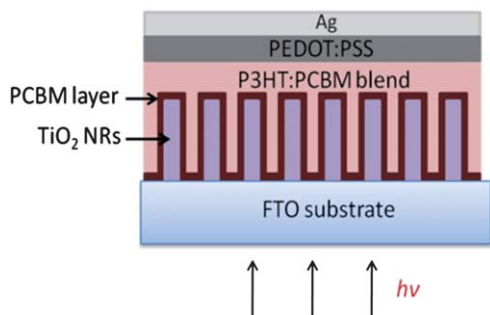
Fig. 7 Schematic drawing of inverted structure polymer solar cells with TiO$_2$ nanorod array buffer layer. The nanorods stretching into the polymers yield a large interface between the P3HT:PCBM active layer and the TiO$_2$ nanorod array buffer layer.[34]

3.2 TiO$_2$ nanotube array as the buffer layer

3.2.1 Fabrication of TiO$_2$ nanotube array using a ZnO nanorod array as the template. TiO$_2$ nanotubes can be synthesized through anodization of titanium foil in an electrolyte containing fluoride ions, which is a well-known method that can readily create oriented TiO$_2$ nanotubes.[35–38] However, the anodization method is incapable of growing the nanotubes on a substrate other than titanium foil. Attempts with a glass substrate by first depositing titanium film and then carrying out an anodization have been demonstrated to be non-ideal in producing a high quality TiO$_2$ nanotube array. To some extent, this drawback has limited the application of the TiO$_2$ nanotube arrays to photovoltaic devices, which specifically require a transparent conductive electrode. The template method is an indirect way to create nanotubes. This can be shown by the fabrication of oriented TiO$_2$ nanotubes based on the ZnO nanorod array that serves as the template for the coating of the TiO$_2$ film and is then removed *via* a treatment in acid solution.[39] The TiO$_2$ nanotubes produced in this way were employed in our study to act as the buffer layer in a polymer solar cell with inverted structure.

3A three-step procedure was carried out to prepare the TiO$_2$ nanotube array for specific use in inverted structure solar cells.[40] (1) *Pre-treatment of substrate*: the ITO glass substrate was cleaned and soaked in an aqueous solution containing 0.1 M (NH$_4$)$_2$TiF$_6$ and 0.2 M H$_3$BO$_3$ for 30 nm for the formation of a layer of TiO$_2$ thin film ~30 nm in thickness on the substrate. The fabrication of such a TiO$_2$ thin film was to ensure a complete separation of the ITO electrode and the polymers that would be prepared later. The TiO$_2$-coated ITO substrate was then spin-coated with a ZnO sol that was formed by 0.6 M Zn(CH$_3$COO)$_2$·H$_2$O dissolved in 2-methoxyethanol/monoethanolamine. This processing results in the formation of a ~50 nm thick seed layer of ZnO on the TiO$_2$ film. The substrate finally underwent a thermal treatment at 300 °C for 10 min to achieve crystalline films. (2) *Growth of ZnO nanorod array*: the pre-treated substrate was immersed in an aqueous solution that contains 0.015 M Zn(NO$_3$)$_2$ and 0.0015 M hexamethylenetetramine at 95 °C for 2 h to grow a ZnO nanorod array. After growth, the substrate with ZnO nanorod array film was rinsed with DI-water and dried with compressed air. (3) *Obtainment of TiO$_2$ nanotubes*: TiO$_2$ nanotubes were obtained by first depositing a layer of TiO$_2$ thin film on the ZnO nanorods by soaking the ZnO nanorod-coated substrate in a precursor solution of TiO$_2$ containing 0.0075 M (NH$_4$)$_2$TiF$_6$ and 0.2 M H$_3$BO$_3$ in water for ~1.5 h. The substrate, on which a film of ZnO nanorod array coated with TiO$_2$ had been formed, was then transferred to a 0.5 M H$_3$BO$_3$ solution to allow the dissolution of the ZnO core, eventually leading to the formation of oriented TiO$_2$ nanotubes on the ITO glass substrate. A consequent thermal treatment at 400 °C for 1 h was performed to achieve crystalline TiO$_2$ nanotubes with the anatase phase.[40]

In the procedure described above, the deposition process of TiO$_2$ on the ZnO nanorods can be represented by the following formula[39,41]

$$TiF_6^{2-} + 2H_2O \rightarrow TiO_2 + 6F^- + 4H^+ \tag{1}$$
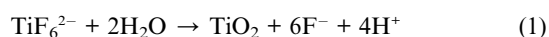
And the dissolution process of ZnO can be outlined as follows:

$$H_3BO_3 + 4H^+ + 4F^- \rightarrow BF_4^- + H_3O^+ + 2H_2O \quad (2)$$

$$ZnO + 2H_3O^+ \rightarrow Zn^{2+} + 3H_2O \quad (3)$$
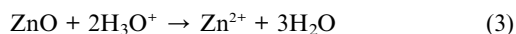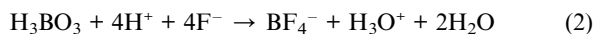
Fig. 8 shows the SEM observation of the as-prepared ZnO nanorods and TiO$_2$ nanotubes. The ZnO nanorods are well grown on the ITO glass substrate in identical orientation vertical to the substrate. The coating of TiO$_2$ on the ZnO nanorods is quite uniform, resulting in well-structured TiO$_2$ nanotubes after the ZnO core is removed. The diameter of each TiO$_2$ nanotube is about 20–30 nm and the length is ~150 to 200 nm. Fig. 8c illustrates the procedure of ZnO nanorod template-based fabrication of TiO$_2$ nanotubes. Energy dispersive X-ray (EDX) analysis shown in Fig. 8d displays the composition evolution of the film from ZnO to TiO$_2$, indicating a successful removal of the ZnO nanorod template and the formation of TiO$_2$ nanotubes.

3.2.2 Enhancing solar cell performance with TiO$_2$ nanotubes for buffer layer.

The TiO$_2$ nanotubes produced with the template method were studied for their performance as the buffer layer in an inverted structure polymer solar cell. The ZnO nanorod array was also studied as reference. The process for the fabrication of polymer solar cells is similar to what is described in Section 3.1.2 and the details can be found elsewhere.[40] Shown in Fig. 9 are the I–V curves of the solar cells using ZnO nanorods and TiO$_2$ nanotubes as the buffer layer, respectively. The photovoltaic parameters are summarized in Table 3. It can be seen that the efficiency of 3.32% for the solar cell with TiO$_2$ nanotube buffer layer is significantly higher than that of 1.19% obtained for the cell with ZnO nanorod buffer layer. Such an efficiency is also slightly higher than 3.21% that was achieved by the cell with TiO$_2$ nanorod buffer layer (see Section 3.1). Summarizing these results, it can be seen that, among the nanostructures discussed in this paper (thin film, nanorods and nanotubes), the use of nanotubes as the buffer layer has been demonstrated to be able to maximally boost the efficiency of an inverted structure solar cell. Likely, this can be attributed to the fact that the nanotubes feature a larger specific surface area than either the thin film or
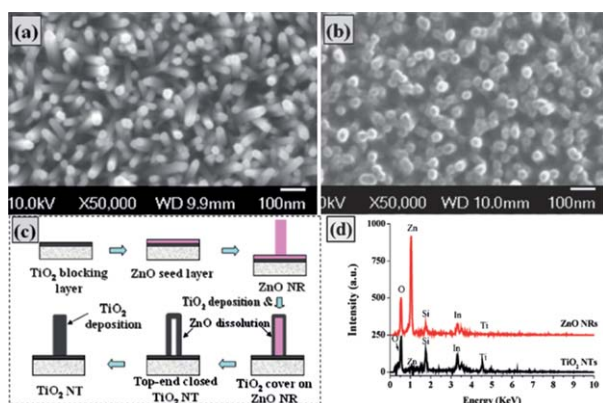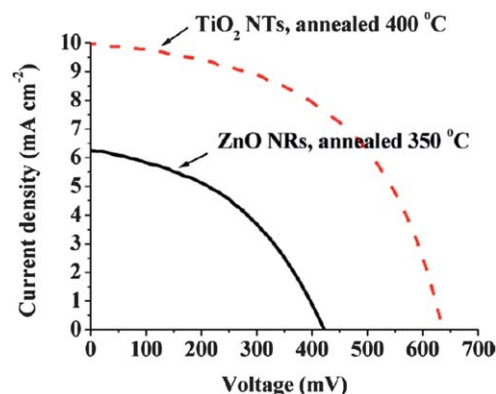
Fig. 9 I–V curves of inverted structure solar cells employing ZnO nanorod or TiO$_2$ nanotube buffer layer.[40]

Table 3 Photovoltaic performance of inverted structure solar cells using ZnO nanorods or TiO$_2$ nanotubes for the buffer layer[40]

Sample (buffer layer)	V_{oc}/mV	J_{sc}/mA cm^{-2}	FF (%)	η (%)
ZnO nanorods (annealed at 350 °C for 1 h)	432	6.28	43.76	1.19
TiO$_2$ nanotubes (annealed at 400 °C for 1 h)	646	9.95	51.60	3.32

the nanorods. In other words, the nanotubes may establish a larger interface between the polymers and the buffer layer compared with the thin film or the nanorods. This is in agreement with our hypothesis (i.e., the second possibility in Section 3.1.3) that the enhanced solar cell performance arises from the branch structure of the nanorod or nanotube array, which stretches into the polymer layers and results in a large interface between the polymers and the buffer layer. Such a large interface may facilitate the electron transport from the PCBM to the buffer layer and thus improve the electron collection of the solar cell.

In Fig. 9 and Table 3, one can also see that the efficiency of 1.19% achieved by ZnO nanorods is much lower than the 3.21% for TiO$_2$ nanorods and the 2.79% for TiO$_2$ thin film (Table 2). This is possibly because that the TiO$_2$ thin film which is pre-coated on the ITO glass is damaged during the growth of ZnO nanorods in an alkaline solution, leading to an incomplete separation of the polymers and the ITO film. This may to some extent explain the noticeably low open circuit voltage and short circuit current shown in Fig. 9 and Table 3 for the cell with ZnO nanorod buffer layer. Such an incomplete separation problem does not happen to the solar cell with TiO$_2$ nanotube array as the buffer layer since the exposed ITO film gets recovered during the deposition of TiO$_2$ to form nanotubes.

4. Conclusions

Oxide nanowires may be utilized to enhance solar cell performance. However, they benefit the dye-sensitized solar cells and inverted structure polymer solar cells in different ways. In dye-sensitized solar cells, the oxide nanowires play the role of the backbone of the photoelectrode film for dye adsorption and,

Fig. 8 SEM images of ZnO nanorod array (a) and TiO$_2$ nanotubes (b). (c) Schematic drawing of the ZnO nanorod array-based template method for the fabrication of TiO$_2$ nanotubes. (d) EDX spectra of ZnO nanorods and TiO$_2$ nanotubes.[40]

moreover, provide direct pathways for electron transport in view of better crystallinity and therefore less electron trapping sites in nanowires than in a nanoparticle film. The electron transport through such direct pathways may importantly suppress charge recombination in dye-sensitized solar cells that occurs between the photogenerated electrons in oxide and the oxidized redox species in electrolyte. However, compared with nanoparticles, the nanowires serving as the photoelectrode film have an obvious disadvantage in offering sufficient surface area for dye adsorption, and therefore the nanowire-based dye-sensitized solar cells present much lower efficiency than those based on nanoparticles. Our study indicates that such a shortcoming of nanowires can be compensated to a great extent by adopting a hybrid structure photoelectrode that consists of nanoparticles dispersed in the nanowire array. Such a hybrid structure photoelectrode may simultaneously provide both large surface area for dye adsorption and direct pathways for electron transport, resulting in a solar cell efficiency enhancement by more than two times compared with the photoelectrode comprised of nanoparticles or nanowires alone in the case of ZnO.

In inverted structure polymer solar cells, the oxide nanowires can serve as the cathode buffer layer and make a contribution to solar cell performance in two aspects. One is that the single crystalline nanowires can transport the photogenerated electrons more efficiently than a polycrystalline thin film. Therefore, the solar cell with a nanowire buffer layer may have higher electron collecting efficiency than that with a thin film buffer layer. The other aspect is that the branch structure of the nanowire array stretching into the polymer layers may yield a larger interface between the polymers and the buffer layer than what a thin film does. Such a large interface may facilitate the electron transport from the PCBM polymer to the buffer layer and thus reduce the probability of photogenerated electrons in the PCBM (electron-acceptor material) being recombined with the holes in P3HT (electron-donor material). Our study supports the second possibility more since, while being used as the cathode buffer layer, the nanotubes demonstrate the highest efficiency over the thin film and nanowires.

However, the role of oxide nanowires serving as the buffer layer in inverted structure solar cells seems to need further study to get better understanding. There are still a lot of uncertainties that may affect the solar cell performance. For example, the surface hydrophilicity of the nanowires and the dispersion density of the nanowire array would affect the degree of polymer penetration into the nanowire array film during the operation of spin-coating. This is directly related to the contact between the polymer and the buffer layer. The area of interface between the polymer and buffer layer and the transport of electrons from the polymer to the buffer layer would be largely determined by the quality of such contact. In addition, the use of a nanowire array for the buffer layer may possibly lead to an incomplete covering of the ITO electrode. A pre-coating of a thin film may be adopted to avoid such a problem, however this would also increase the complexity of the interface between the nanowire buffer layer and the ITO film and probably diminish the electron transport. The dimensions of nanowires are also an aspect that needs to be optimized to avoid light scattering so as to maximize the enhancement effect of the nanowire buffer layer.

References

1 Y. Li, F. Qian, J. Xiang and C. M. Lieber, *Mater. Today*, 2006, **9**, 18–27.
2 Y. Cui, Z. Zhong, D. Wang, W. U. Wang and C. M. Lieber, *Nano Lett.*, 2003, **3**, 149–152.
3 J. P. Colinge, C. W. Lee, A. Afzalian, N. D. Akhavan, R. Yan, I. Ferain, P. Razavi, B. O'Neill, A. Blake and M. White, *Nat. Nanotechnol.*, 2010, **5**, 225–229.
4 W. Lu and C. L. M. Lieber, *Nat. Mater.*, 2007, **6**, 841–850.
5 M. A. Zimmler, F. Capasso, S. Müller and C. Ronning, *Semicond. Sci. Technol.*, 2010, **25**, 024001.
6 J. C. Johnson, H. J. Choi, K. P. Knutsen, R. D. Schaller, P. Yang and R. J. Saykally, *Nat. Mater.*, 2002, **1**, 106–110.
7 A. B. Greytak, C. J. Barrelet, Y. Li and C. M. Lieber, *Appl. Phys. Lett.*, 2005, **87**, 151103.
8 M. H. Huang, S. Mao, H. Feick, H. Yan, Y. Wu, H. Kind, E. Weber, R. Russo and P. Yang, *Science*, 2001, **292**, 1897.
9 J. Y. Zhang, P. J. Li, H. Sun, X. Shen, T. S. Deng, K. T. Zhu, Q. F. Zhang and J. L. Wu, *Appl. Phys. Lett.*, 2008, **93**, 021116.
10 M. H. Sun, Q. F. Zhang and J. L. Wu, *J. Phys. D: Appl. Phys.*, 2007, **40**, 3798–3802.
11 H. Sun, Q. F. Zhang and J. L. Wu, *Nanotechnology*, 2006, **17**, 2271–2274.
12 Y. Cui, Q. Wei, H. Park and C. M. Lieber, *Science*, 2001, **293**, 1289.
13 J. H. Ahn, S. J. Choi, J. W. Han, T. J. Park, S. Y. Lee and Y. K. Choi, *Nano Lett.*, 2010, **10**, 2934–2938.
14 C. K. Chan, H. Peng, G. Liu, K. McIlwrath, X. F. Zhang, R. A. Huggins and Y. Cui, *Nat. Nanotechnol.*, 2007, **3**, 31–35.
15 C. K. Chan, X. F. Zhang and Y. Cui, *Nano Lett.*, 2008, **8**, 307–309.
16 E. Hosono, T. Kudo, I. Honma, H. Matsuda and H. Zhou, *Nano Lett.*, 2009, **9**, 1045–1051.
17 L. Mai, L. Xu, C. Han, X. Xu, Y. Luo, S. Zhao and Y. Zhao, *Nano Lett.*, 2010, **10**, 4750–4755.
18 M. Law, L. E. Greene, J. C. Johnson, R. Saykally and P. Yang, *Nat. Mater.*, 2005, **4**, 455–459.
19 V. Sivakov, G. Andrä, A. Gawlik, A. Berger, J. Plentz, F. Falk and S. Christiansen, *Nano Lett.*, 2009, **9**, 1549–1554.
20 E. Garnett and P. Yang, *Nano Lett.*, 2010, **10**, 1082–1087.
21 Q. F. Zhang and G. Z. Cao, *Nano Today*, 2011, **6**, 91–109.
22 S. Yodyingyong, Q. F. Zhang, K. Park, C. S. Dandeneau, X. Y. Zhou, D. Triampo and G. Z. Cao, *Appl. Phys. Lett.*, 2010, **96**, 073115.
23 Q. Li, V. Kumar, Y. Li, H. Zhang, T. J. Marks and R. P. H. Chang, *Chem. Mater.*, 2005, **17**, 1001–1006.
24 Q. F. Zhang, T. R. Chou, B. Russo, S. A. Jenekhe and G. Z. Cao, *Angew. Chem., Int. Ed.*, 2008, **47**, 2402–2406.
25 Q. F. Zhang, C. S. Dandeneau, X. Y. Zhou and G. Z. Cao, *Adv. Mater.*, 2009, **21**, 4087–4108.
26 K. Keis, J. Lindgren, S. E. Lindquist and A. Hagfeldt, *Langmuir*, 2000, **16**, 4688–4694.
27 T. P. Chou, Q. F. Zhang and G. Z. Cao, *J. Phys. Chem. C*, 2007, **111**, 18804–18811.
28 L. M. Chen, Z. Hong, G. Li and Y. Yang, *Adv. Mater.*, 2009, **21**, 1434–1449.
29 R. Po, C. Carbonera, A. Bernardi and N. Camaioni, *Energy Environ. Sci.*, 2011, **4**, 285–310.

30 Y. Liang, Z. Xu, J. Xia, S. T. Tsai, Y. Wu, G. Li, C. Ray and L. Yu, *Adv. Mater.*, 2010, **22**, E135–E138.
31 P. de Bruyn, D. Moet and P. Blom, *Org. Electron.*, 2010, **11**, 1419–1422.
32 P. P. Boix, J. Ajuria, I. Etxebarria, R. Pacios, G. Garcia-Belmonte and J. Bisquert, *J. Phys. Chem. Lett.*, 2011, **2**, 407–411.
33 B. Liu and E. S. Aydil, *J. Am. Chem. Soc.*, 2009, **131**, 3985–3990.
34 J. T. Xi, O. Wiranwetchayan, Q. F. Zhang, Z. Q. Liang, Y. M. Sun and G. Z. Cao, Growth of single-crystalline rutile TiO$_2$ nanorods on fluorine-doped tin oxide glass for organic-inorganic hybrid solar cells. (Unpublished).
35 D. Gong, C. A. Grimes, O. K. Varghese, W. C. Hu, R. S. Singh, Z. Chen and E. C. Dickey, *J. Mater. Res.*, 2001, **16**, 3331–3334.
36 G. K. Mor, K. Shankar, M. Paulose, O. K. Varghese and C. A. Grimes, *Nano Lett.*, 2006, **6**, 215–218.
37 G. K. Mor, O. K. Varghese, M. Paulose, K. Shankar and C. A. Grimes, *Sol. Energy Mater. Sol. Cells*, 2006, **90**, 2011–2075.
38 J. M. Macak, H. Tsuchiya and P. Schmuki, *Angew. Chem., Int. Ed.*, 2005, **44**, 2100–2102.
39 C. K. Xu, P. H. Shin, L. L. Cao, J. M. Wu and D. Gao, *Chem. Mater.*, 2010, **22**, 143–148.
40 S. Yodyingyong, X. Y. Zhou, Q. F. Zhang, D. Triampo, J. T. Xi, K. Park, B. Limketkai and G. Z. Cao, *J. Phys. Chem. C*, 2010, **114**, 21851–21855.
41 S. Deki, S. Iizuka, A. Horie, M. Mizuhata and A. Kajinami, *Chem. Mater.*, 2004, **16**, 1747–1750.